Journal of Computational Physics **157,** 588–617 (2000)
doi:10.1006/jcph.1999.6393, available online at http://www.idealibrary.com on IDEAL®

A Wavenumber Based Extrapolation and Interpolation Method for Use in Conjunction with High-Order Finite Difference Schemes

Christopher K. W. Tam and Konstantin A. Kurbatskii

Department of Mathematics, Florida State University, Tallahassee, Florida 32306-4510
E-mail: tam@math.fsu.edu

Received February 2, 1999; revised July 29, 1999

The errors incurred in using extrapolation and interpolation in large scale computations are analyzed and quantified in the wavenumber space. If a large extrapolation stencil is used, the errors in the low wavenumbers can be significantly reduced. However, the errors in the high wavenumbers are, at the same time, greatly increased. The opposite is true if the stencil size is reduced. Based on the wavenumber analysis, an optimized extrapolation and interpolation method is proposed. The optimization is carried out over a selected band of wavenumbers. It is known that extrapolation often leads to numerical instability. The instability is the result of large error amplification in the high wavenumber range. To reduce the tendency to trigger numerical instability, it is proposed that an extra constraint be imposed on the optimized extrapolation method. The added constraint aims to reduce error amplification over the high wavenumbers. Numerical examples are provided to illustrate that accurate and stable numerical results can be obtained in large scale simulation using a high-order finite difference scheme and the proposed optimized extrapolation method. When the same problems are recomputed using the familiar high-order polynomials extrapolation method in the Lagrange form, in one case the numerical results are plagued by large errors and ultimately instability. In another problem, it is found that the use of the Lagrange polynomials extrapolation method would lead immediately to numerical instability.

Key Words: extrapolation; interpolation; wavenumber analysis; high-order finite difference.

1. INTRODUCTION

Presently, interpolation and extrapolation are widely used in large scale scientific computing. Some computation schemes, in particular a subset of essentially nonoscillatory schemes, have incorporated extrapolation as an intrinsic part of the method (see Refs. [1–4]).

0021-9991/00 $35.00

Others, e.g., Refs. [5–8], used extrapolation to extend the values of the solution from the interior to the boundary of the computation domain to form inflow and outflow boundary conditions. Hayder and Turkel [9], on the other hand, employed extrapolation to implement radiation boundary conditions for computational acoustics. When composite grids are used in the solution of a scientific problem, there are occasions when some fringe points cannot be updated by the general computation scheme. Steger and Benek [10] suggested that in such a situation the solution at these points may be determined by extrapolation.

Many finite difference and finite volume schemes currently used in large scale computing rely on interpolation as a key element of the algorithm. In multigrid methods, interpolation is often used in the mesh to mesh transfer of the solution between the coarse and fine grids, e.g., Refs. [11–14]. Some investigators prefer to use overset grids in their computation, Refs. [8, 15–18]. In using overset grids, an interpolation procedure is invariably called upon to perform data transfer in the region with overlapping mesh points. In the multidomain method, very often a nonaligned grid is the most convenient grid for the problem. In formulating their staggered grid spectral method, Kopriva and Kolias [19] employed interpolation to resolve the nonaligned grid problem.

Using high-order polynomials is, by far, the most popular method for interpolation and extrapolation. For convenience, we will use the Lagrange form of polynomial extrapolation and interpolation In this work, we will only consider extrapolation and interpolation on a regular mesh. Also, we will assume that a high-order finite difference or finite volume scheme is used. To maintain comparable accuracy, a large stencil (nearly the same size as the finite difference or finite volume scheme) is used for interpolation and extrapolation. Suppose a N-point computation stencil with a mesh spacing Δx is used to extrapolate the values of a function $f(x)$ to the point $x_0 + \eta\Delta x$ ($\eta < 1$) as shown in Fig. 1. Without loss of generality, we will let x_0 be the first stencil point. The Lagrange polynomials formed by N mesh points are

$$\ell_k^{(N)}(x) = \prod_{\substack{j=0 \\ j\neq k}}^{N-1} \frac{(x - x_j)}{(x_k - x_j)}, \qquad k = 0, 1, 2, \ldots, (N-1). \tag{1}$$

The extrapolated value of f at $\eta\Delta x$ is then given by

$$f(x_0 + \eta\Delta x) \simeq \sum_{k=0}^{N-1} f_k \ell_k^{(N)}(x_0 + \eta\Delta x), \tag{2}$$

where $f_k = f(x_k)$, $k = 0, 1, 2, \ldots, (N-1)$, are the values of f at the mesh points.

It is interesting that most text books on numerical analysis discuss interpolation at great length but rarely mention extrapolation. Conte and de Boor [20], after an in-depth presentation of interpolation, wrote that if the interpolation point went outside the stencil it became extrapolation and "extrapolation should only be used with great caution." The warning is proper and real. It is a well known fact in scientific computing that extrapolation often

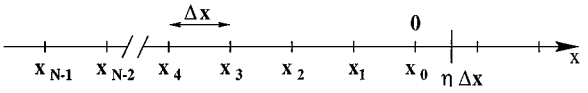

FIG. 1. Schematic diagram showing an N-point extrapolation stencil at spacing Δx and the extrapolation point at $\eta\Delta x$.

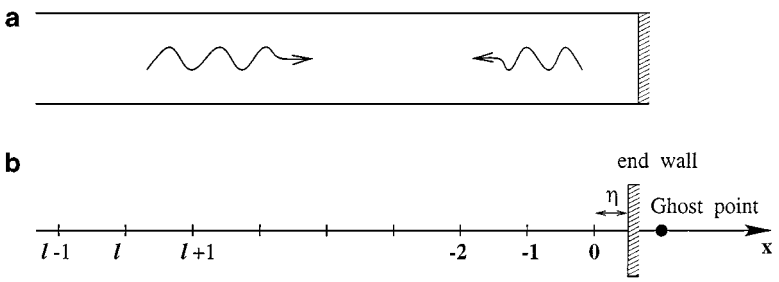

FIG. 2. Schematic diagram showing (a) the propagation and reflection of one-dimensional acoustic waves in a long duct with a closed end, (b) the computational mesh and ghost point.

leads to numerical instability. This being the case, one is, however, surprised to find that the literature has little to say why extrapolation causes numerical instability. Not knowing the reason is, perhaps, why no new extrapolation scheme, that is both accurate and less prone to instability, has been proposed in recent years.

The main objective of this work is to examine extrapolation and interpolation from a wavenumber standpoint. It will be shown that the errors incurred in extrapolation and interpolation can be determined precisely in wavenumber space. By knowing the errors quantitatively, it is possible to adjust the coefficients of the scheme to make the extrapolation and interpolation procedure accurate over a large band of wavenumbers.

To provide a concrete example of numerical instability arising from the use of the Lagrange polynomials extrapolation method and to show that such an instability can be suppressed by using an improved method, let us consider the problem of acoustic wave propagation and reflection in a long tube (one-dimensional) with closed ends (see Fig. 2). For convenience, dimensionless variables with respect to length scale Δx (the mesh spacing), velocity scale a_∞ (the speed of sound), time scale $\frac{\Delta x}{a_\infty}$, density scale ρ_∞ (ambient gas density), and pressure scale $\rho_\infty a_\infty^2$ will be used. It will be assumed that the right end wall is not at a mesh point but at a distance η ($\eta < 1.0$) from the last mesh point $\ell = 0$ as shown in Fig. 2. The governing equations are the linearized momentum and energy equations of a compressible fluid. Let u and p be the fluid velocity and pressure. The dimensionless governing equations are

$$\frac{\partial u}{\partial t} + \frac{\partial p}{\partial x} = 0 \tag{3}$$

$$\frac{\partial p}{\partial t} + \frac{\partial u}{\partial x} = 0. \tag{4}$$

The wall boundary condition is

$$u = 0 \qquad \text{at} \quad x = \eta. \tag{5}$$

Suppose one solves the problem by finite difference approximation in x on a mesh as shown in Fig. 2. To provide a highly accurate solution with small dispersion error, let us use the standard 7-point central difference scheme (6th orders scheme) to approximate the x-derivative. The semi-discretized system derived from (3) and (4) is

$$\frac{du_\ell}{dt} + \sum_{j=-3}^{3} a_j p_{\ell+j} = 0 \tag{6}$$

$$\frac{dp_\ell}{dt} + \sum_{j=-3}^{3} a_j u_{\ell+j} = 0, \tag{7}$$

where ℓ is the mesh point index and the a_j $(-3 \le j \le 3)$ are the stencil coefficients. Near the wall where a 7-point central difference scheme cannot fit, backward difference stencils are used. Since the wall is not at a mesh point, the value of u at the wall may be obtained by extrapolation using the values of u at the nearest seven mesh points. Suppose the Lagrange polynomials are used for extrapolation. The wall boundary condition (5) becomes

$$\sum_{k=0}^{6} u_{-k} \ell_k^{(7)}(\eta) = 0. \tag{8}$$

To enforce the boundary condition in the finite difference computation, the ghost point method of Tam and Dong [21] may be used. The ghost point method was designed for use in conjunction with a high-order finite difference scheme. In this method, a ghost value of pressure at the ghost point, $\ell = 1$, is introduced. The ghost value is chosen so that (8) is satisfied at every time level of the computation.

In the Appendix, it will be shown that the above discrete system is numerically unstable. The system supports a single boundary instability mode with time dependence $e^{-i\omega t}$ where $\omega = \omega_r + i\omega_i$ is the complex frequency. The angular frequency, ω_r, and the temporal growth rate, ω_i, of the instability can be determined analytically. They are given in Fig. 3 as a function of η (the location of the wall from the first mesh point). The instability can, of course, be determined computationally as well by using a time marching scheme such as the 4th-order Runge–Kutta scheme (with a very small time step). Figure 4 shows the computed value of p at $\ell = -3$ as a function of time. By measuring the oscillation period and amplitude, the angular frequency and growth rate of the boundary instability can be found. The numerically determined values of ω_r and ω_i are in good agreement with the analytical values of the Appendix. They are shown in Fig. 3.

The observed numerical instability of the acoustic wave problem is due entirely to the use of the Lagrange extrapolation formula (8). It will be shown later that by using an improved extrapolation scheme, there is no numerical instability. A hint that the boundary instability can be eliminated may be found in Fig. 3b. This figure clearly indicates that even when the Lagrange polynomials extrapolation formula is used, the system is unstable only when η is larger than 0.42. So it is highly plausible that one could design a new extrapolation scheme capable of extending the stable region all the way to $\eta = 1.0$.

Numerical instability inevitably requires a mechanism to amplify the numerical solution unintentionally. The difference between an amplified solution and the true solution is the error. In other words, a mechanism that introduces large error could lead to numerical instability. From this point of view, a necessary condition for being able to design a more stable extrapolation scheme is a way to assess quantitatively the error of the scheme. Furthermore, if a method to control the maximum error is found, then by implementing the method to limit the maximum error of an extrapolation scheme, it would then be possible to diminish the prospect of encountering numerical instability in large scale computing.

For the Lagrange polynomials method, there is no known way to calculate the errors quantitatively. To assess error, the standard approach suggests that one assume that Δx is small and then make use of the Taylor series expansion of Eq. (2) to provide an order of magnitude error estimate. It can be shown by truncating the Taylor series that the method

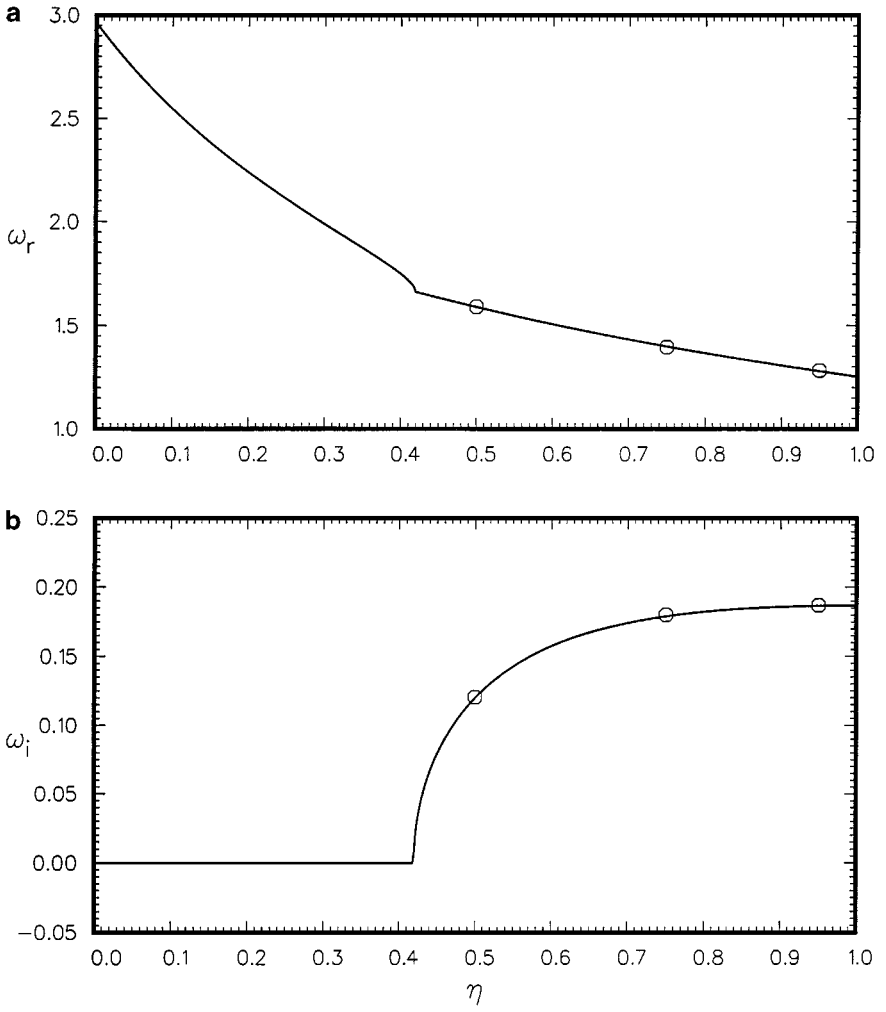

FIG. 3. Boundary instability induced by numerical extrapolation using Lagrange polynomials. (a) Real part of unstable frequency versus the distance of extrapolation to the wall, (b) the imaginary part. —, analytical; ○, numerical simulation.

has an error of order $(\Delta x)^{(N-1)}$ if N mesh points are used for extrapolation. Unfortunately, this order of magnitude error estimate is not quantitative enough to be useful.

The rest of this paper is as follows. In Section 2, a way to determine the errors involved in extrapolation from the values of a function at N mesh points to a point at η is presented. This analysis is carried out in wavenumber space. An optimized extrapolation procedure is then developed. The purpose of the optimization is to keep the extrapolation error minimum over a large band in wavenumber space. It will be shown that extrapolation could introduce large error in the high wavenumbers or short waves. This large error is the mechanism which amplifies the solution leading to numerical instability. Thus numerical instability is primarily associated with the short waves. It is proposed to add an additional constraint in the optimization process to keep the overall error smaller in the high wavenumbers. In this way, the tendency for extrapolation to trigger numerical instability is greatly reduced. In Section 3 a wavenumber analysis of interpolation is performed. Based on the results of this

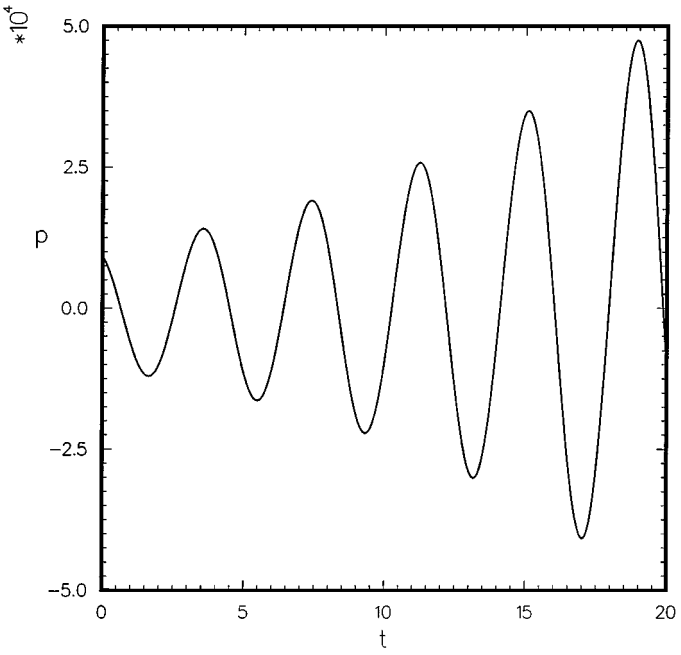

FIG. 4. Computed pressure time-history at $l = -3$. The wall is located at $\eta = 0.45$.

analysis, an optimized interpolation method is developed. In Section 4, an example on the use of the newly developed extrapolation and interpolation method in large scale computing is provided. This example offers strong evidence that the new extrapolation method, when used in conjunction with high-order finite difference schemes, can yield accurate and stable numerical solutions.

2. WAVENUMBER ANALYSIS OF EXTRAPOLATION

We will assume that the function $f(x)$, to be extrapolated, has a Fourier transform $\tilde{f}(\alpha)$ where α is the wavenumber. $f(x)$ is related to $\tilde{f}(\alpha)$ by the Fourier inverse transform formula,

$$f(x) = \int_{-\infty}^{\infty} \tilde{f}(\alpha) e^{i\alpha x}\, d\alpha. \tag{9}$$

For convenience, we will denote the absolute value and argument of $\tilde{f}(\alpha)$ by A and ϕ, i.e.,

$$A(\alpha) = |\tilde{f}(\alpha)| \qquad \text{and} \qquad \phi(\alpha) = \arg[\tilde{f}(\alpha)]$$

so that (9) may be rewritten as

$$f(x) = \int_{-\infty}^{\infty} A(\alpha) e^{i(\alpha x + \phi(\alpha))}\, d\alpha. \tag{10}$$

A simple interpretation of (10) is that $f(x)$ is made up of a superposition of simple waves with wavenumber α and amplitude $A(\alpha)$. Recently, a wavenumber analysis of large

stencil finite difference schemes (see Tam and Webb [22] and Tam [23]) has shown that finite difference schemes are accurate only over a limited band of low wavenumbers. We will consider designing an extrapolation scheme that is highly accurate over a similar wavenumber range, say, $-\kappa \le \alpha\Delta x \le \kappa$. Our goal is for the extrapolation scheme to work well for very general functions. For this purpose, it will be sufficient to consider waves with unit amplitude over the desired band of wavenumbers. Thus from (10), the simple wave with wavenumber α to be considered is

$$f_\alpha(x) = e^{i[\alpha x + \phi(\alpha)]}. \tag{11}$$

The total effect on the function $f(x)$ will, of course, have to be weighed by the amplitude function $A(\alpha)$.

2.1. *Extrapolation Error in Wavenumber Space*

Now, instead of the Lagrange polynomials extrapolation formula (2), we will use the general formula

$$f(x_0 + \eta\Delta x) = \sum_{j=0}^{(N-1)} S_j f(x_j), \qquad x_j = x_0 - j\Delta x, \tag{12}$$

where S_j ($j = 0, 1, 2, \ldots, (N-1)$) are the stencil coefficients. $S_j = \ell_j^{(N)}(x_0 + \eta\Delta x)$ if the Lagrange polynomials are used. We will define the local extrapolation error, $E_{\text{local}}(\eta, \kappa, \alpha\Delta x, N)$, as the square of the absolute value of the difference between the left and right side of (12) when the single Fourier component of (11) is substituted into the formula. Note: the dependence on the parameter κ will become clear later.

$$\begin{aligned} E_{\text{local}}(\eta, \kappa, \alpha\Delta x, N) &= \left| e^{i[\alpha(x_0+\eta\Delta x)+\phi]} - \sum_{j=0}^{N-1} S_j e^{i[\alpha(x_0 - j\Delta x)+\phi]} \right|^2 \\ &= \left| e^{i\eta\alpha\Delta x} - \sum_{j=0}^{N-1} S_j e^{-ij\alpha\Delta x} \right|^2. \end{aligned} \tag{13}$$

It is to be noted that $E_{\text{local}}(\eta, \kappa, -\alpha\Delta x, N) = E_{\text{local}}(\eta, \kappa, \alpha\Delta x, N)$, so that E_{local} is an even function of $\alpha\Delta x$.

The integrated error over the band of wavenumbers from $\alpha\Delta x = 0$ to $\alpha\Delta x = \kappa$ is

$$E = \int_0^\kappa \left| e^{i\eta\alpha\Delta x} - \sum_{j=0}^{N-1} S_j e^{-ij\alpha\Delta x} \right|^2 d(\alpha\Delta x). \tag{14}$$

One desired property of extrapolation is that the error is zero if the function is a constant (i.e., zero wavenumber). The extrapolation error in this special case is obtained by setting $\alpha = 0$ in (13). We will, therefore, restrict the choice of S_j by the condition

$$E_{\text{local}}(\eta, \kappa, 0, N) = \left| 1 - \sum_{j=0}^{N-1} S_j \right|^2 = 0. \tag{15}$$

Now, we will choose S_j, the coefficients of extrapolation formula (12), so that E is a minimum subjected to the constraint (15). This constrained optimization problem can easily be handled by the method of Lagrange multiplier. The Lagrangian function may be defined as

$$L = \int_0^{\kappa} \left| e^{i\eta y} - \sum_{j=0}^{N-1} S_j e^{-ijy} \right|^2 dy + \lambda \left(\sum_{j=0}^{N-1} S_j - 1 \right). \tag{16}$$

The coefficients S_j and the parameter λ are found by solving the linear system,

$$\frac{\partial L}{\partial S_j} = 0 \qquad \text{or} \qquad \mathrm{Re}\left[-\int_0^{\kappa} e^{ijy} \left(e^{i\eta y} - \sum_{k=0}^{N-1} S_k e^{-iky} \right) dy \right] + \frac{\lambda}{2} = 0 \tag{17}$$

$$\frac{\partial L}{\partial \lambda} = 0 \qquad \text{or} \qquad \sum_{j=0}^{N-1} S_j - 1 = 0. \tag{18}$$

The algebraic system of (17) and (18) leads to the linear matrix equation

$$\begin{bmatrix}
\kappa & \sin\kappa & \frac{\sin 2\kappa}{2} & \frac{\sin 3\kappa}{3} & \frac{\sin 4\kappa}{4} & \cdot & \cdot & \cdot & \frac{\sin[(N-1)\kappa]}{N-1} & \frac{1}{2} \\
\sin\kappa & \kappa & \sin\kappa & \frac{\sin 2\kappa}{2} & \frac{\sin 3\kappa}{3} & \cdot & \cdot & \cdot & \frac{\sin[(N-2)\kappa]}{N-2} & \frac{1}{2} \\
\frac{\sin 2\kappa}{2} & \sin\kappa & \kappa & \sin\kappa & \frac{\sin 2\kappa}{2} & \cdot & \cdot & \cdot & \frac{\sin[(N-3)\kappa]}{N-3} & \frac{1}{2} \\
\frac{\sin 3\kappa}{3} & \frac{\sin 2\kappa}{2} & \sin\kappa & \kappa & \sin\kappa & \cdot & \cdot & \cdot & \frac{\sin[(N-4)\kappa]}{N-4} & \frac{1}{2} \\
\cdot & \cdot & \cdot & \cdot & \cdot & \cdot & \cdot & \cdot & \cdot & \cdot \\
\cdot & \cdot & \cdot & \cdot & \cdot & \cdot & \cdot & \cdot & \cdot & \cdot \\
\frac{\sin[(N-1)\kappa]}{N-1} & \frac{\sin[(N-2)\kappa]}{N-2} & \cdot & \cdot & \cdot & \cdot & \frac{\sin 2\kappa}{2} & \sin\kappa & \kappa & \frac{1}{2} \\
1 & 1 & 1 & \cdot & \cdot & \cdot & 1 & 1 & 1 & 0
\end{bmatrix}$$

$$\cdot \begin{bmatrix} S_0 \\ S_1 \\ S_2 \\ S_3 \\ \cdot \\ \cdot \\ S_{N-1} \\ \lambda \end{bmatrix} = \begin{bmatrix} \frac{\sin(\eta\kappa)}{\eta} \\ \frac{\sin(\eta+1)\kappa}{\eta+1} \\ \frac{\sin(\eta+2)\kappa}{\eta+2} \\ \frac{\sin(\eta+3)\kappa}{\eta+3} \\ \cdot \\ \cdot \\ \frac{\sin(\eta+N-1)\kappa}{\eta+N-1} \\ 1 \end{bmatrix}. \tag{19}$$

For a given η and N, the coefficients of the extrapolation formula (12), S_j, can be found by solving (19). κ is a free parameter, which can be selected to offer the best overall results. Obviously κ has a significant influence on the values of S_j and hence the local error

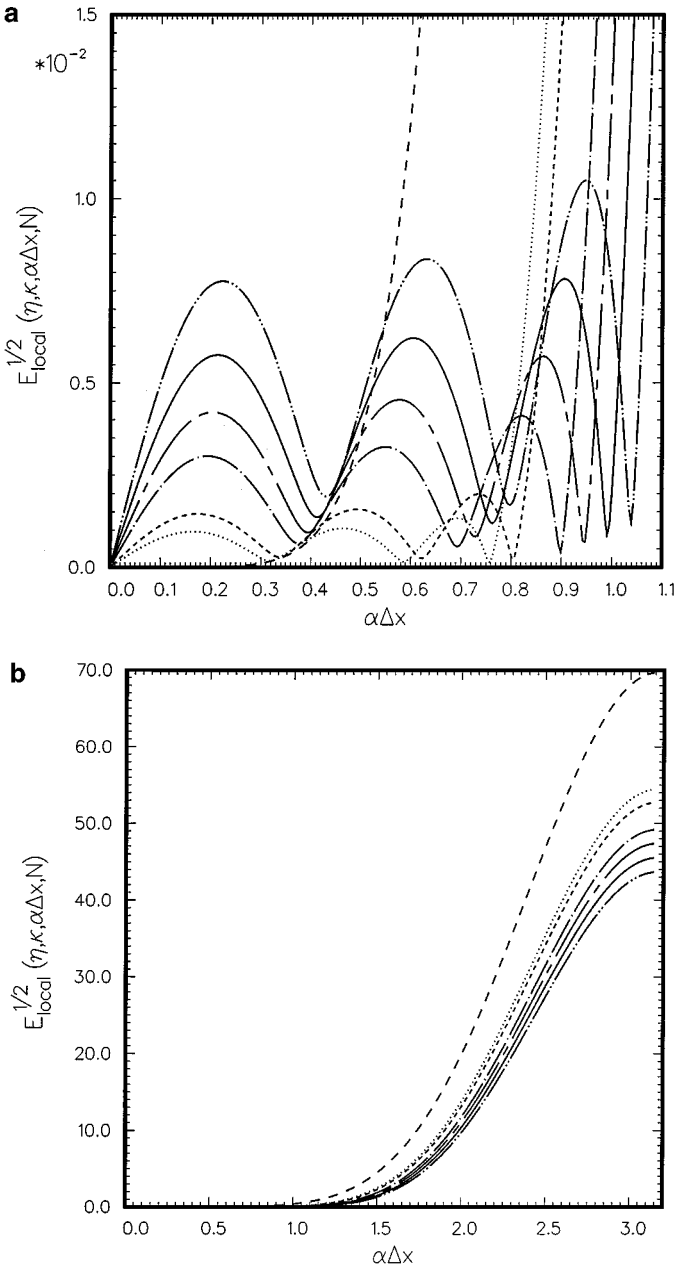

FIG. 5. (a) Dependence of local error on wavenumber over the long wave range for the case $\eta = 0.75$, $N = 7$. . . . , $\kappa = 0.8$; - - -, $\kappa = 0.85$; —·—·—, $\kappa = 0.95$; — - — - —, $\kappa = 1.0$; —, $\kappa = 1.05$; —·—·—·—, $\kappa = 1.1$; — — —, Lagrange polynomials extrapolation. (b) Dependence of local error on wavenumber (full range) for the case $\eta = 0.75$, $N = 7$. . . . , $\kappa = 0.8$; - - -, $\kappa = 0.85$; —·— ·—, $\kappa = 0.95$; — - — - —, $\kappa = 1.0$; —, $\kappa = 1.05$; —·—·—·—, $\kappa = 1.1$; — — —, Lagrange polynomials extrapolation.

$E_{\text{local}}(\eta, \kappa, \alpha\Delta, N)$. Figure 5a shows the dependence of $E_{\text{local}}^{1/2}$ on wavenumber $\alpha\Delta x$ in the case $\eta = 0.75$ and $N = 7$ for several values of κ. This figure is typical of other values of η and N. Plotted in this figure also is the local error of the Lagrange polynomials extrapolation. It is readily seen that the Lagrange polynomials extrapolation is very accurate for

low wavenumbers. For wavenumbers larger than $\alpha\Delta x = 0.6$ or wavelengths shorter than $10.5\Delta x$, the local error is quite large. Many finite difference schemes used in large scale computations and simulations, especially those designed for solving wave propagation problems (see Refs. [22, 23]), can resolve waves longer than 8 mesh spacings or $\alpha\Delta x \leq 0.85$. It would, therefore, be incompatible to use the Lagrange polynomials extrapolation with these schemes. On the other hand, the local error of the optimized extrapolation is larger at very low waveumbers. But the error is not excessive even for $\alpha\Delta x$ as large as 0.85 or wavelength equal to 8 mesh spacings. It has much less error over the intermediate wavenumber range.

Figure 5b shows the distribution of local error for the same values of η and N as Fig. 5a but over the full range of wavenumbers, i.e., $0 \leq \alpha\Delta x \leq \pi$. For high wavenumbers, in particular at $\alpha\Delta x = \pi$ or the grid-to-grid oscillations, the local error is extremely large for the Lagrange polynomials extrapolation. In the case of the optimized extrapolation, the error, depending on the choice of κ, is less. Nevertheless, it is still large and unacceptable. For this reason, it is important that the function to be extrapolated be sufficiently smooth and free of high wavenumber components.

To examine the variation of extrapolation error on η, let

$$E_{\max}(\eta, \kappa, N) = \max_{0 \leq \alpha\Delta x \leq 0.85} E_{\text{local}}(\eta, \kappa, \alpha\Delta x, N). \tag{20}$$

This is the maximum error incurred in the extrapolation process if the function involved has a Fourier spectrum confined to the range $\alpha\Delta x \leq 0.85$. Figure 6 shows the dependence of $E_{\max}$ on η for the case $N = 7$. If the Lagrange polynomials extrapolation is used, the maximum error grows rapidly with η, the distance of extrapolation. $E_{\max}$ for the optimized

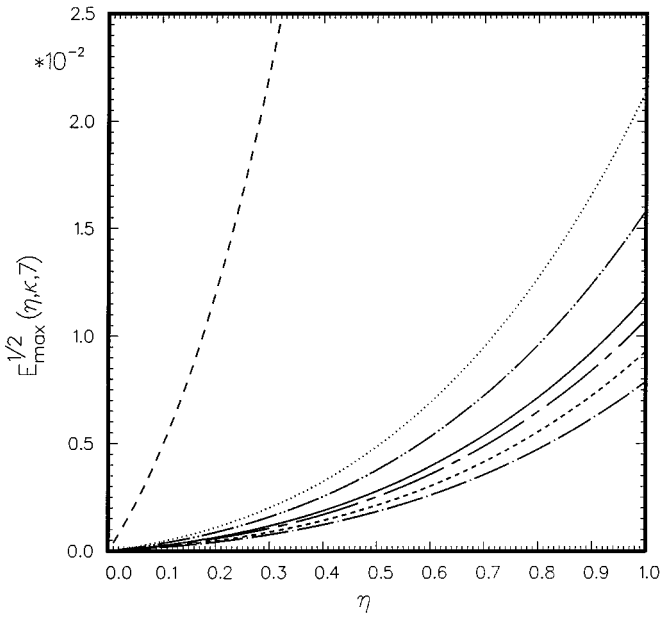

FIG. 6. Dependence of maximum local error (maximized over $0 \leq \alpha\Delta x \leq 0.85$) on η for the case $N = 7$. . . . , $\kappa = 0.8$; - - -, $\kappa = 0.85$; —·—·—, $\kappa = 0.95$; — - — - —, $\kappa = 1.0$; —, $\kappa = 1.05$; —·—·—·—, $\kappa = 1.1$; — — —, Lagrange polynomials extrapolation.

scheme is much less. For $\kappa = 0.85$, $E_{\max}^{1/2}$ reaches a value of 0.0092 at $\eta = 1.0$. In most situations, η is less than 1.0 and the error is accordingly much smaller.

An extensive investigation of the local error distribution for the values of η from 0 to 1 and $N = 5$, 6, 7, and 8 has been carried out. It is found that the local error remains low over $0 \le \alpha \Delta x \le 0.85$ if κ is taken to be 0.85. Based on this numerical study, it is recommended that the parameter κ be assigned the value 0.85 when used in connection with large scale high-order finite difference computation. In the remainder of this paper κ is set equal to 0.85 unless stated otherwise.

2.2. *Additional Constraint for Optimized Extrapolation*

Figure 5b reveals that even for the optimized extrapolation, the error for high wavenumbers, particularly for $\alpha \Delta x$ near π, can be excessive. What this means is that if a large scale computation contains high wavenumber components, these components can be greatly amplified by the extrapolation process. We believe that it is this numerical error amplification mechanism that is responsible for the well known numerical instability widely encountered in the use of extrapolation. From this point of view, it would be desirable to keep the local error at $\alpha \Delta x = \pi$ and the high wavenumbers smaller. This can be done by imposing an additional constraint on the optimization process by which the extrapolation coefficients, S_j, are found. Suppose it is desired to fix the extrapolated error of the function at $\alpha \Delta x = \pi$ to be a prescribed value, say, $h(\eta)$. That is, we impose the additional condition,

$$e^{i(\alpha x_0 + \phi)} \left[\sum_{j=0}^{N-1} S_j e^{-ij\pi} - h(\eta) \right] = 0. \tag{21}$$

The first term of (21) is equal to the extrapolated value of the simple wave function $f_\alpha(x)$ of (11) at $\alpha \Delta x = \pi$. It is usually much larger than $e^{i\eta\pi}$ and hence, for all intents and purposes, it is equal to the squared root of the local error. By specifying the function $h(\eta)$, one imposes the maximum error allowed at $\alpha \Delta x = \pi$. Needless to say, the choice of $h(\eta)$ would affect the extrapolation error over the low wavenumber range. Thus a compromise must be made to allow a slight increase in the extrapolation error over the low wavenumber range in exchange for a reduction in error for $\alpha \Delta x$ in the neighborhood of π. Extensive numerical experiments have been carried out to find a good selection of $h(\eta)$. We find that the simple choice of a linear function of η,

$$h(\eta) = 1.0 + 19\eta \tag{22}$$

works quite well.

Upon including (21) as an additional constraint, the Lagrangian function to be minimized may be taken to be

$$\mathcal{L} = \int_0^\kappa \left| e^{i\eta y} - \sum_{j=0}^{N-1} S_j e^{-ijy} \right|^2 dy + \lambda \left(\sum_{j=0}^{N-1} S_j - 1 \right) + \mu \left(\sum_{j=0}^{N-1} S_j e^{-ij\pi} - h(\eta) \right). \tag{23}$$

The conditions for minimization are

$$\frac{\partial \mathcal{L}}{\partial S_j} = 0, \quad j = 0, 1, 2, \ldots, (N-1), \qquad \frac{\partial \mathcal{L}}{\partial \lambda} = 0, \qquad \frac{\partial \mathcal{L}}{\partial \mu} = 0. \tag{24}$$

Equation (24) may be recast into a matrix system similar to (19). The matrix equation has the form

$$\begin{bmatrix}
\kappa & \sin\kappa & \frac{\sin 2\kappa}{2} & \frac{\sin 3\kappa}{3} & \frac{\sin 4\kappa}{4} & \cdot & \cdot & \frac{\sin[(N-1)\kappa]}{N-1} & \frac{1}{2} & \frac{1}{2} \\
\sin\kappa & \kappa & \sin\kappa & \frac{\sin 2\kappa}{2} & \frac{\sin 3\kappa}{3} & \cdot & \cdot & \frac{\sin[(N-2)\kappa]}{N-2} & \frac{1}{2} & -\frac{1}{2} \\
\frac{\sin 2\kappa}{2} & \sin\kappa & \kappa & \sin\kappa & \frac{\sin 2\kappa}{2} & \cdot & \cdot & \frac{\sin[(N-3)\kappa]}{N-3} & \frac{1}{2} & \frac{1}{2} \\
\frac{\sin 3\kappa}{3} & \frac{\sin 2\kappa}{2} & \sin\kappa & \kappa & \sin\kappa & \cdot & \cdot & \frac{\sin[(N-4)\kappa]}{N-4} & \frac{1}{2} & -\frac{1}{2} \\
\cdot & \cdot & \cdot & \cdot & \cdot & \cdot & \cdot & \cdot & \cdot & \cdot \\
\cdot & \cdot & \cdot & \cdot & \cdot & \cdot & \cdot & \cdot & \cdot & \cdot \\
\frac{\sin[(N-1)\kappa]}{N-1} & \frac{\sin[(N-2)\kappa]}{N-2} & \frac{\sin[(N-3)\kappa]}{N-3} & \cdot & \cdot & \cdot & \cdot & \kappa & \frac{1}{2} & (-1)^{N-1}\frac{1}{2} \\
1 & 1 & 1 & 1 & 1 & \cdot & \cdot & 1 & 0 & 0 \\
1 & -1 & 1 & -1 & 1 & \cdot & \cdot & (-1)^{N-1} & 0 & 0
\end{bmatrix}$$

$$\cdot \begin{bmatrix} S_0 \\ S_1 \\ S_2 \\ S_3 \\ \cdot \\ \cdot \\ S_{N-1} \\ \lambda \\ \mu \end{bmatrix} = \begin{bmatrix} \frac{\sin(\eta\kappa)}{\eta} \\ \frac{\sin(\eta+1)\kappa}{\eta+1} \\ \frac{\sin(\eta+2)\kappa}{\eta+2} \\ \frac{\sin(\eta+3)\kappa}{\eta+3} \\ \cdot \\ \cdot \\ \frac{\sin(\eta+N-1)\kappa}{\eta+N-1} \\ 1 \\ h(\eta) \end{bmatrix}. \tag{25}$$

Matrix (25) can be solved readily. Once the S_j's are found, one can again assess the local error $E_{\text{local}}(\eta, \kappa, \alpha\Delta x, N)$ as before. Figure 7a shows the variation of $E_{\text{local}}^{1/2}$ with wavenumbers $\alpha\Delta x$ for $\kappa = 0.85$, $N = 7$, at four values of η. As can be seen, for a computation with a spatial resolution of 8 mesh spacings per wavelength or $\alpha\Delta x \leq 0.8$, the maximum extrapolation error is less than 1.5%. For comparison purpose, the local error for the Lagrange polynomials extrapolation is also plotted. It is evident that for $\alpha\Delta x > 0.6$, the error is huge. Figure 7b shows an identical plot but covers the entire range of wavenumbers. Near $\alpha\Delta x = \pi$, there is significant difference in the errors between the two extrapolation procedures. For instance, for $\eta = 1.0$ the Lagrange polynomials method has an error about six times larger than that of the optimized scheme. We, therefore, expect that the improved optimized scheme is less likely to induce numerical instability.

Figures 8a–9b provide similar information as Figs. 7a and 7b at stencil size of 5 and 8. They are included here to offer numerical data on the effect of using a smaller or larger extrapolation stencil. Generally speaking, the use of a larger stencil reduces the error in the low wavenumber range but increases the error at high wavenumbers. This is the type of trade-off information that would help one to decide the proper stencil size to use in a given situation.

To provide a concrete example that the added constraint in the optimized extrapolation method does reduce numerical instability, the one-dimensional acoustic wave propagation

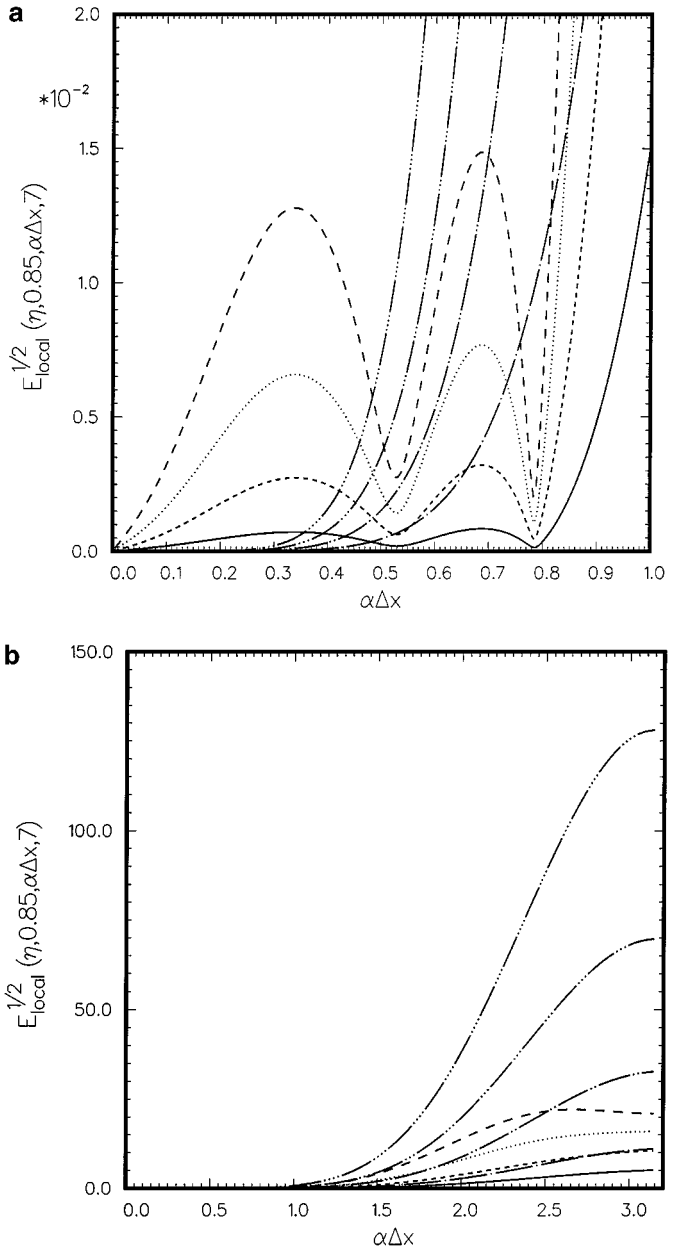

FIG. 7. (a) Local error as a function of the wavenumber using the optimized extrapolation method with an added constraint. $\kappa = 0.85$, $N = 7$.

η	Optimized extrapolation	Lagrange polynomials extrapolation
0.25	—	— · — · —
0.50	- - -	— ·· — ·· —
0.75	· · ·	— · · · — · · · —
1.00	— — —	— · · ·· — · · ·· —

(b) Same as (a) but for wavenumber $0 \leq \alpha\Delta x \leq \pi$.

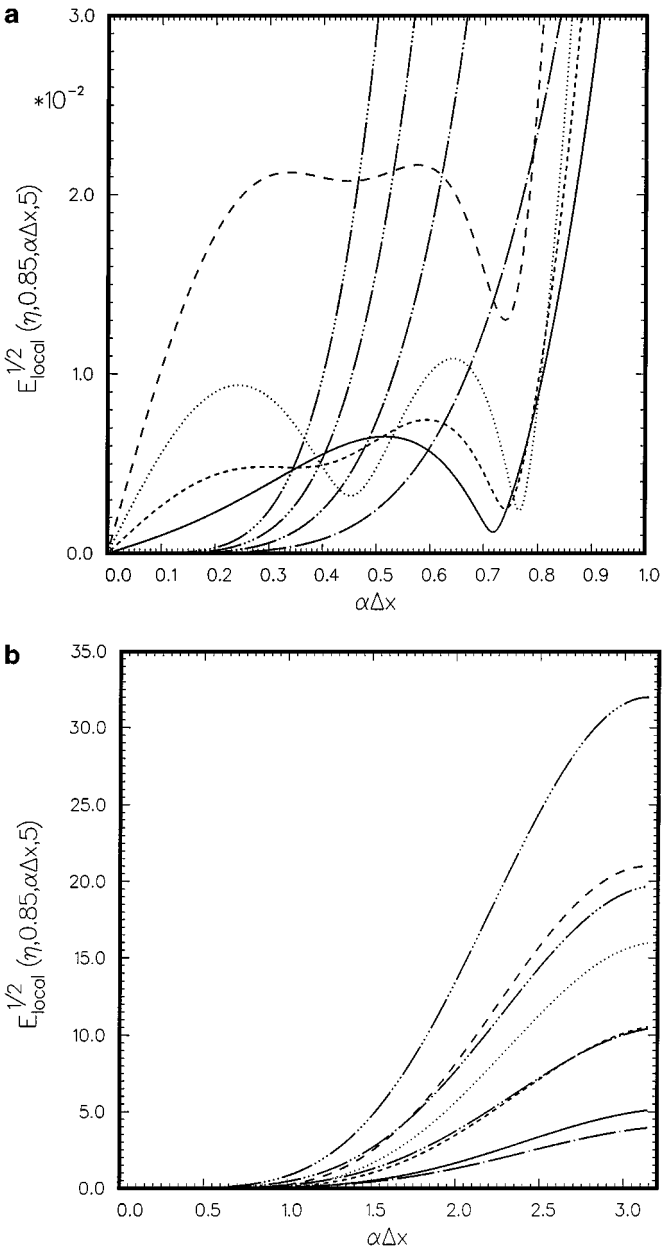

FIG. 8. (a) Local error as a function of the wavenumber using the optimized extrapolation method with an added constraint. $\kappa = 0.85,\ N = 5$.

η	Optimized extrapolation	Lagrange polynomials extrapolation
0.25	—	— · — · —
0.50	- - -	— ·· — ·· —
0.75	· · ·	— · · · — · · · —
1.00	— — —	— · · ·· — · · ·· —

(b) Same as (a) but for wavenumber $0 \le \alpha \Delta x \le \pi$.

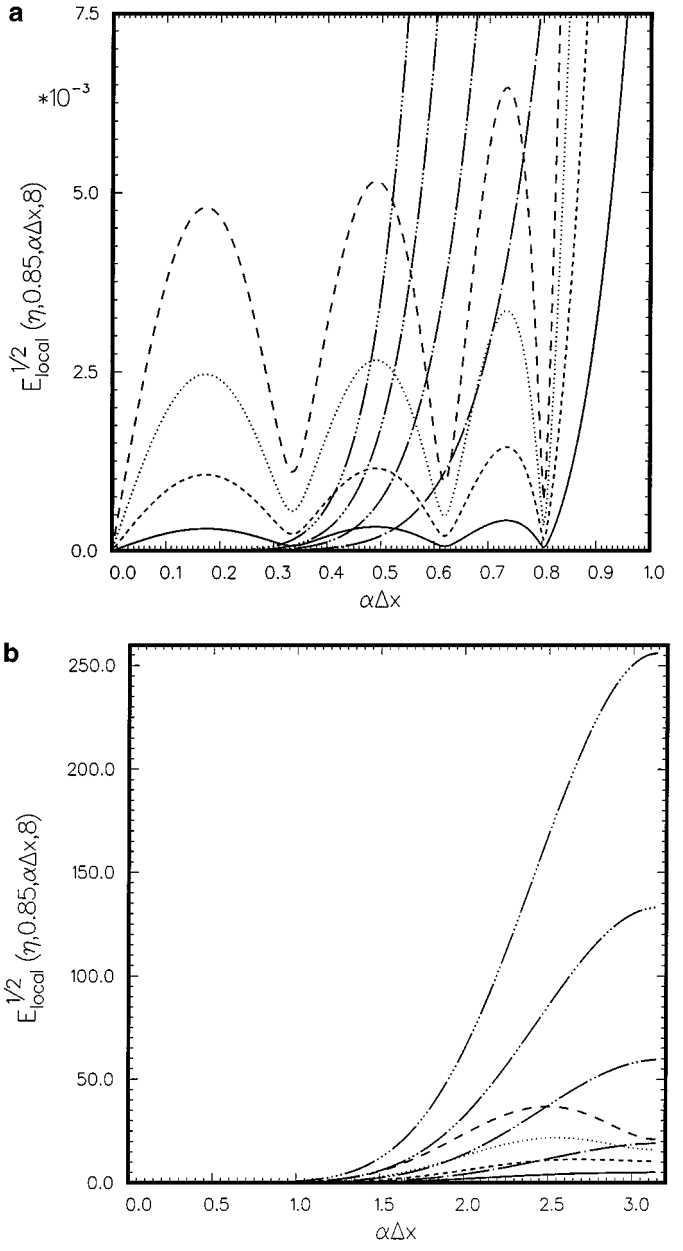

FIG. 9. (a) Local error as a function of the wavenumber using the optimized extrapolation method with an added constraint. $\kappa = 0.85$, $N = 8$.

η	Optimized extrapolation	Lagrange polynomials extrapolation
0.25	—	— · — · —
0.50	- - -	— ·· — ·· —
0.75	· · ·	— · · · — · · · —
1.00	— — —	— · · ·· — · · ·· —

(b) Same as (a) but for wavenumber $0 \leq \alpha \Delta x \leq \pi$.

and reflection problem discussed in the introductory section is again considered. Now let the extrapolation of u to the wall location at $x = \eta$ (see Eq. (5)) be carried out by the optimized extrapolation scheme with an added constraint instead of the Lagrange polynomials extrapolation; i.e., replacing (8) by

$$\sum_{j=0}^{6} u_{-j} S_j(\eta) = 0. \tag{26}$$

The boundary instability problem is recalculated following the procedure in the Appendix. The analytic results as well as direct numerical simulations indicate that there is no boundary instability. In other words, the optimized scheme with the additional constraint has effectively eliminated the boundary instability altogether. This example should lend confidence that the new extrapolation method has less tendency to induce numerical instability which is an extremely desirable characteristic. It is to be noted that by using the optimized scheme alone, without the added constraint, the problem remains unstable, although with a lower growth rate. The additional constraint to reduce amplification at high wavenumbers is essential to numerical stability.

3. OPTIMIZED INTERPOLATION

Interpolation is a subject that is treated in great depth in most books on numerical analysis. In addition to high-order polynomials, piecewise polynomials, splines, and trigonometric functions are often used. They generally give good results. However, a survey of the commonly used textbooks indicates that interpolation error is seldom discussed quantitatively. Most books use the Taylor series truncation term as an error indicator. But such a term cannot be easily translated into useful quantitative information.

In this section, we will perform a wavenumber analysis of interpolation error and, at the same time, formulate an optimized interpolation procedure. Interpolation is generally a numerically stable operation incurring relatively less error than extrapolation. For this reason, one can only expect a relatively small improvement by the optimized interpolation as compared to using, for example, the more familiar Lagrange polynomials interpolation or polynomial interpolation under some other famous names.

3.1. *Wavenumber Analysis of Interpolation*

Consider an N-point interpolation stencil as shown in Fig. 10. Let x_0 be the first point of the stencil. The other stencil points are located at $x_j = x_0 - j\Delta x$. Suppose the interpolation point is in the Kth interval of the stencil at a distance of $\eta\Delta x$ to the right of x_K. In other words, the value of a function at the interpolation point $x_i = x_0 - K\Delta x + \eta\Delta x$ is to be found from the known values at x_j $(j = 0, 1, 2, \ldots, (N-1))$.

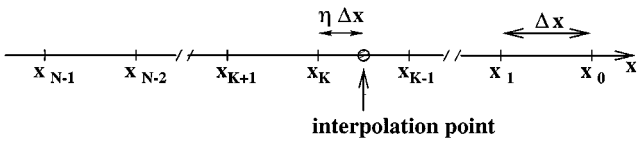

FIG. 10. An N-point interpolation stencil showing the location of the interpolation point.

The interpolation formula is

$$f(x_0 - (K-\eta)\Delta x) = \sum_{j=0}^{N-1} S_j f(x_j). \tag{27}$$

As in the case of extrapolation, we will define the local interpolation error, $\bar{E}_{\text{local}}$, as the square of the absolute value of the difference between the left and the right sides of (27) when the single Fourier component of (11) is substituted into the formula, i.e.,

$$\begin{aligned}\bar{E}_{\text{local}} &= \left| e^{i[\alpha(x_0 - K\Delta x + \eta\Delta x)+\phi]} - \sum_{j=0}^{N-1} S_j e^{i[\alpha(x_0 - j\Delta x)+\phi]} \right|^2 \\ &= \left| e^{-i(K-\eta)\alpha\Delta x} - \sum_{j=0}^{N-1} S_j e^{-ij\alpha\Delta x} \right|^2. \end{aligned} \tag{28}$$

Now, the local error $\bar{E}_{\text{local}}(\eta, \kappa, \alpha\Delta x, N, K)$ depends on the parameter K as well as η, κ, $\alpha\Delta x$, and N; the parameters involved in extrapolation.

The integrated error over the band of wavenumbers from $\alpha\Delta x = 0$ to $\alpha\Delta x = \kappa$ is

$$\bar{E} = \int_0^{\kappa} \left| e^{-i(K-\eta)\alpha\Delta x} - \sum_{j=0}^{N-1} S_j e^{-ij\alpha\Delta x} \right|^2 d(\alpha\Delta x). \tag{29}$$

We will now choose S_j so that $\bar{E}$ is a minimum subjected to the condition that there is no error for the zero wavenumber component. The zero wavenumber condition may be written as

$$\bar{E}_{\text{local}}(\eta, \kappa, 0, K, N) = \left| 1 - \sum_{j=0}^{N-1} S_j \right|^2 = 0. \tag{30}$$

The Lagrangian function to be minimized is

$$\bar{L} = \int_0^{\kappa} \left| e^{-i(K-\eta)y} - \sum_{k=0}^{N-1} S_k e^{-iky} \right|^2 dy + \lambda \left(\sum_{k=0}^{N-1} S_k - 1 \right). \tag{31}$$

The conditions for minimum are

$$\frac{\partial \bar{L}}{\partial S_j} = 0, \qquad \frac{\partial \bar{L}}{\partial \lambda} = 0, \qquad j = (0, 1, 2, \ldots, (N-1)). \tag{32}$$

Equation (32) yields the algebraic equations

$$\sum_{j=0}^{N-1} S_j \frac{\sin(\ell - j)\kappa}{(\ell - j)} + \frac{\lambda}{2} = \frac{\sin(\ell - K + \eta)\kappa}{(\ell - K + \eta)}, \qquad \ell = 0, 1, 2, \ldots, (N-1) \tag{33a}$$

$$\sum_{j=0}^{N-1} S_j = 1. \tag{33b}$$

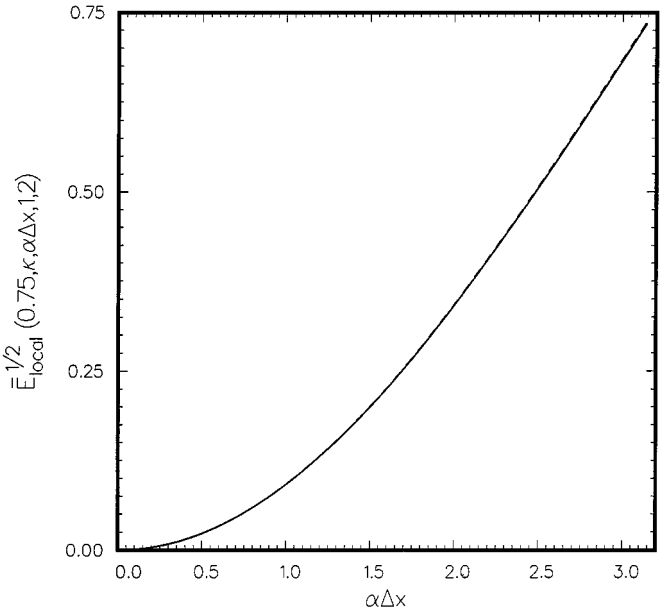

FIG. 11. Local interpolation error as a function of wavenumber. $N=2$, $K=1$, $\eta=0.75$. . . . , $\kappa=0.85$; - - -, $\kappa=0.9$; —·—·—, $\kappa=0.95$; —·—·—·—, $\kappa=1.0$; —, $\kappa=1.05$; —··—··—, $\kappa=1.1$; — — —, Lagrange polynomials interpolation.

The linear system (33) can be rewritten in a matrix form similar to Eq. (19). The matrix equation can be solved easily to provide the interpolation coefficients, S_j ($j=0, 1, 2, \ldots, (N-1)$).

3.2. *Numerical Results*

The local interpolation error, $\bar{E}_{\text{local}}$, as a function of wavenumber $\alpha\Delta x$ depends on a number of parameters. They are N (the stencil size), K (the interval number), and η (the distance to the mesh point) as well as the free parameter κ. Numerical results are now provided to offer an idea on the magnitude of the error and how it is influenced by the various parameters.

Let us begin with N, the size of the stencil. Figure 11 shows the distribution of $\bar{E}^{1/2}_{\text{local}}$ in wavenumber space for $\eta=0.75$ using only two interpolation points, $N=2$. This is a very special case. The parameter κ appears to have negligible effect on the local error. Also the optimized scheme yields almost identical results as the Lagrange polynomials interpolation. The error is quite large in the high wavenumber range but relatively small at low wavenumbers. We will now keep the interpolation point in the first interval of the stencil, i.e., $K=1$, but allow the stencil size to increase. Figures 12a and 12b show the local error distributions as functions of wavenumber at various values of κ with $N=7$ or seven interpolation points. On comparing with Fig. 11, it is clear that by increasing the size of the stencil, the error in the low wavenumber range drops rapidly. At the same time, the error in the high wavenumbers increases dramatically.

If the interpolation point lies in the interior of a large stencil, one intuitively expects much smaller error than when it is located at the first interval. Figures 13a and 13b show

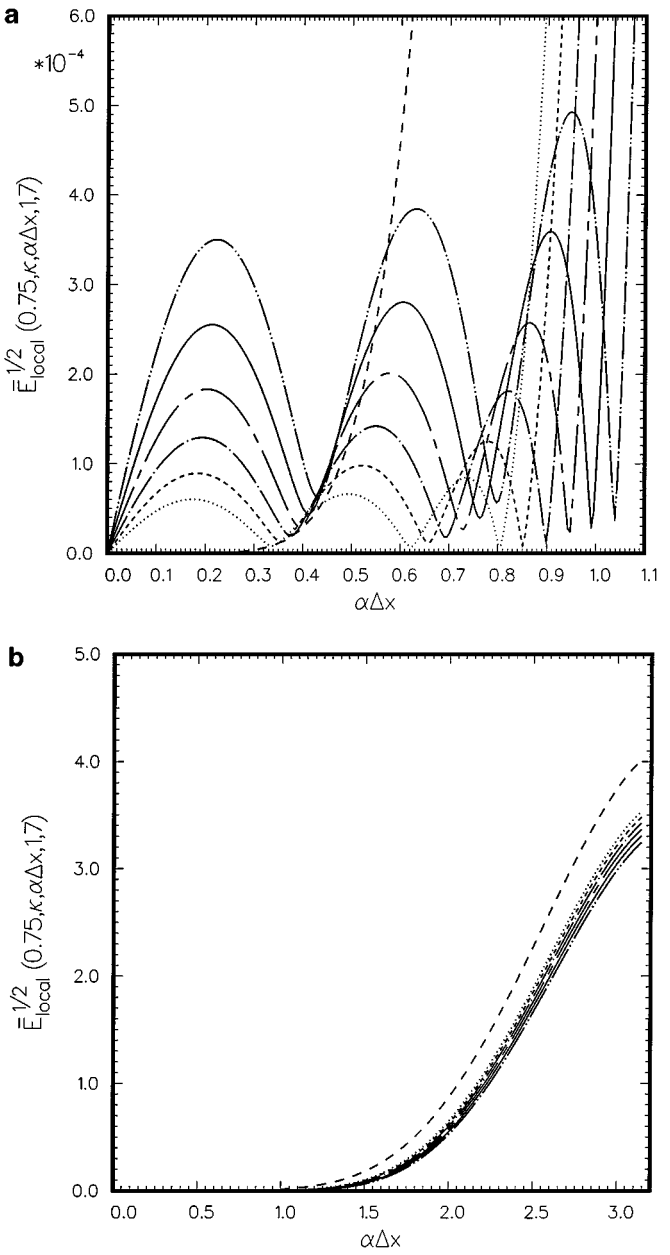

FIG. 12. (a) Local interpolation error as a function of wavenumber. $N = 7$, $K = 1$, $\eta = 0.75$. . . . , $\kappa = 0.85$; - - -, $\kappa = 0.9$; — · — · —, $\kappa = 0.95$; — - — - —, $\kappa = 1.0$; —, $\kappa = 1.05$; — · · — · · —, $\kappa = 1.1$; — — —, Lagrange polynomials interpolation. (b) Same as (a) but for wavenumber $0 \le \alpha\Delta x \le \pi$.

the numerical results for $N = 7$, $\eta = 0.75$, and $K = 2$. Figures 14a and 14b show the corresponding results for $K = 3$. These results completely confirm the intuitive expectation. Over the long wave range, $\alpha\Delta x \le 0.9$, there is hardly any error when the interpolation point lies in the center interval.

We will now consider the effect of the distance of the interpolation point from the stencil point, namely, η. Extensive numerical computation of the local error as η varies with the

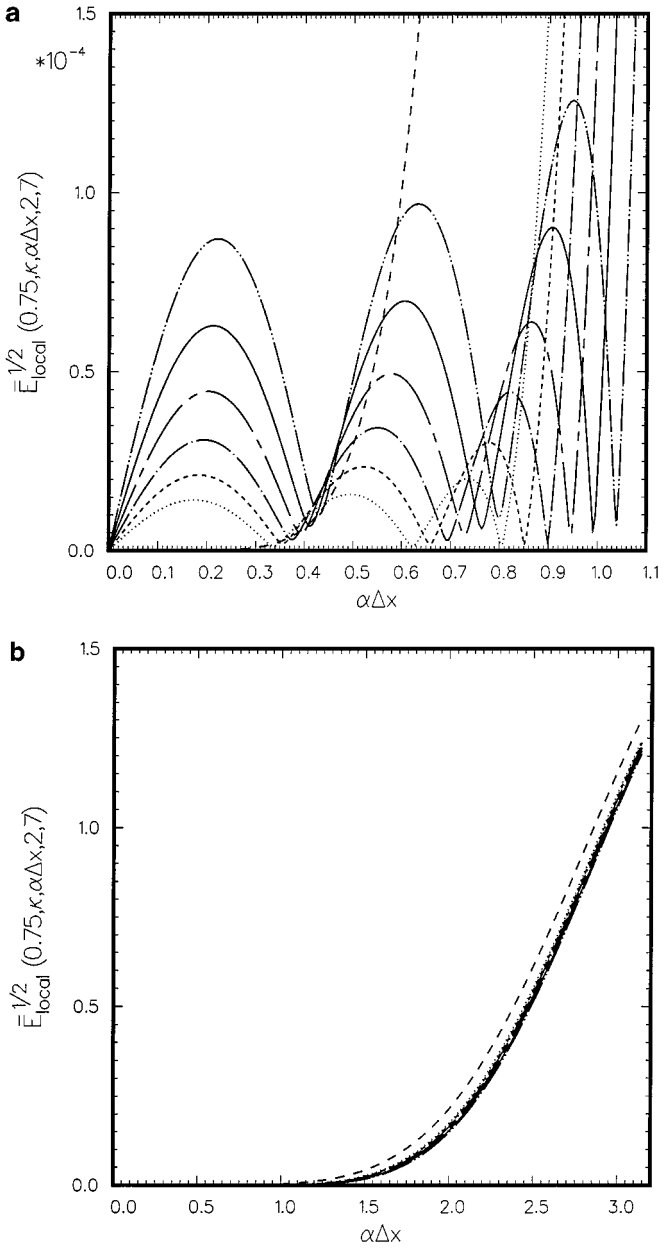

FIG. 13. (a) Local interpolation error as a function of wavenumber. $N = 7$, $K = 2$, $\eta = 0.75$. . . . , $\kappa = 0.85$; - - -, $\kappa = 0.9$; — · — · —, $\kappa = 0.95$; — - — - —, $\kappa = 1.0$; —, $\kappa = 1.05$; — · · — · · —, $\kappa = 1.1$; — — —, Lagrange polynomials interpolation. (b) Same as (a) but for wavenumber $0 \leq \alpha\Delta x \leq \pi$.

other parameters fixed reveals that there is little change in the local error. In other words, η has a relatively small effect on the local error.

Finally, we turn to the free parameter κ. After reviewing and comparing all the numerical results we have, it is our opinion that a good overall choice for this parameter is 1.0. This value of κ provides a large range of low wavenumbers over which the interpolation error is small. At the same time, the error at high wavenumbers is still numerically small. In

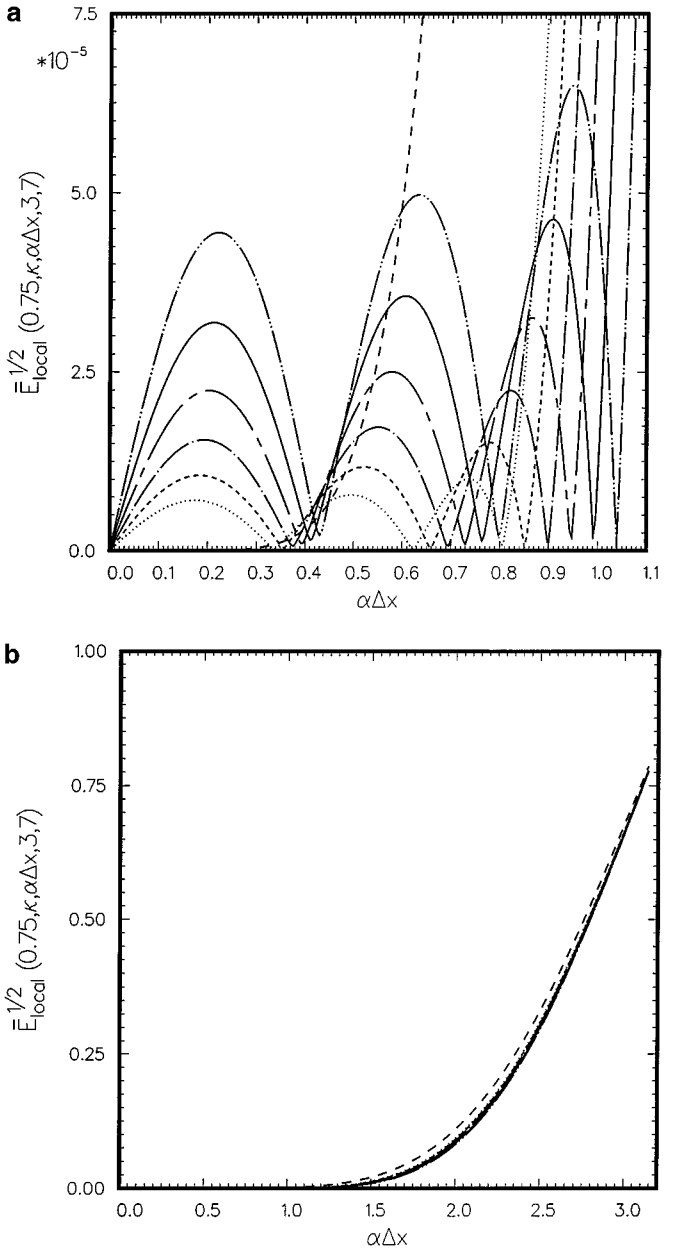

FIG. 14. (a) Local interpolation error as a function of wavenumber. $N = 7$, $K = 3$, $\eta = 0.75$. . . . , $\kappa = 0.85$; - - -, $\kappa = 0.9$; — · — · —, $\kappa = 0.95$; — - — - —, $\kappa = 1.0$; —, $\kappa = 1.05$; — · · — · · —, $\kappa = 1.1$, — — —, Lagrange polynomials interpolation. (b) Same as (a) but for wavenumber $0 \le \alpha\Delta x \le \pi$.

most large scale computations, the high wavenumber components will remain unresolved. They are the spurious numerical waves, which are often suppressed by the inclusion of artificial selective damping or filtering. As a result, the amplitude of the high wavenumber components is small. Any amplification by the interpolation process would still be small. They should not be a concern except in unusual circumstances.

4. NUMERICAL EXAMPLE

As an example on the use of extrapolation and interpolation in large scale computing, we will consider the problem of scattering of plane acoustic waves by a cylinder in two dimensions. Let the diameter of the cylinder be D. The governing equations are the linearized Euler equations. In dimensionless form, they may be written as (with respect to length scale D, velocity scale c (speed of sound), time scale $\frac{D}{c}$, density scale ρ_0, and pressure scale $\rho_0 c^2$),

$$\frac{\partial \mathbf{U}}{\partial t} + \frac{\partial \mathbf{E}}{\partial x} + \frac{\partial \mathbf{F}}{\partial y} = 0, \tag{34}$$

where

$$\mathbf{U} = \begin{bmatrix} \rho \\ u \\ v \\ p \end{bmatrix}, \qquad \mathbf{E} = \begin{bmatrix} u \\ p \\ 0 \\ u \end{bmatrix}, \qquad \mathbf{F} = \begin{bmatrix} v \\ 0 \\ p \\ v \end{bmatrix}.$$

On the surface of the cylinder, the boundary condition is $\mathbf{V} \cdot \mathbf{n} = 0$ where $\mathbf{n}$ is the unit normal to the surface. It can be easily shown that an equivalent form of the boundary condition is

$$\frac{\partial p}{\partial n} = 0. \tag{35}$$

Equation (34) can be discretized on a Cartesian mesh using a high-order finite difference scheme such as the dispersion-relation-preserving scheme, Ref. [22]. The advantage of a high-order scheme is that the numerical dispersion and dissipation error may be minimized. The scattered sound field can be found by time marching the numerical solution to a time periodic state. However, because the cylinder has a curved surface, a special boundary treatment is needed to enforce boundary condition (35). For this purpose, the present authors [24] have extended the ghost point method of Tam and Dong [21] to treat arbitrarily curved wall boundaries. As an illustration of the boundary treatment, consider the curved boundary shown in Fig. 15. First, the boundary curve is approximated by line segments joining the intersection points of the computation mesh and the boundary. For instance, the curved surface between points A and B in Fig. 15 is replaced by a straight line segment. G_2 is a ghost point. A ghost value of pressure is assigned to G_2 to enforce boundary condition (35). The enforcement point is at E; G_2E is perpendicular to AB. Since $\frac{\partial p}{\partial x}$ and $\frac{\partial p}{\partial y}$ are not known except on the mesh points, their values at A and B are found by extrapolation from the points at $(1', 2', 3', 4', 5', 6', 7')$ and $(1, 2, 3, 4, 5, 6, 7)$, respectively. The corresponding values at E are then calculated by interpolation from those at A and B. Once $\frac{\partial p}{\partial x}$ and $\frac{\partial p}{\partial y}$ are found at E, (35) can be enforced readily.

To show the impact of the extrapolation scheme on the computed results of the scattered waves, a computation domain of 320×320 with $\Delta x = \Delta y = \frac{D}{32}$ is used in the solution of the scattering problem. The wavelength of the incoming acoustic waves is equal to $8\Delta x$. The incoming plane acoustic waves are generated by a set of nonhomogeneous radiation boundary conditions developed by Tam, Fang, and Kurbatskii [25] imposed at the boundary region of the computation domain. The nonhomogeneous radiation boundary conditions perform two functions. First, they generate the incoming waves. Then they also allow the

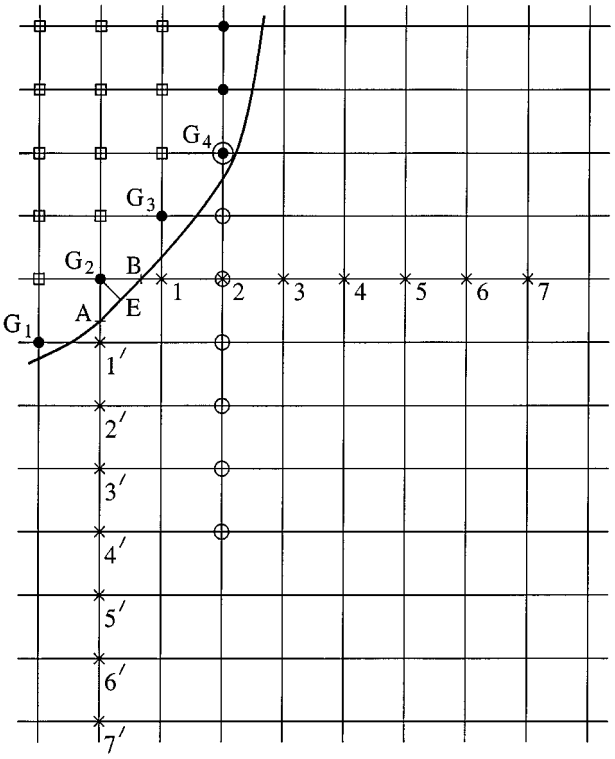

FIG. 15. Cartesian boundary treatment of curved wall surfaces.

scattered waves to exit the boundaries with minimal reflection. The discretized boundary is highly irregular. It becomes a strong source of spurious numerical waves. These waves have short wavelengths or high wavenumbers. To eliminate the spurious waves, artificial selective damping terms (see Refs. [23, 24]) are added to the governing finite difference equations in the boundary region around the cylinder. Because of the special boundary treatment needed to enforce the curved wall boundary condition, the accuracy of the computed scattered wave is influenced by the extrapolation formula used. Figure 16 shows the computed zero pressure contours of the scattered waves at the beginning of a cycle (the 15th cycle from the start of the numerical computation) when the Lagrange polynomials extrapolation is used in the computation. Shown in dotted lines are the zero pressure contours of the exact solution. It is obvious that there are significant differences between the two sets of contours. It is not difficult to understand why there are such large discrepancies. The wavenumber analysis of Section 2 indicates that at 8 mesh points per wavelength, the Lagrange polynomials extrapolation method would give rise to large errors. Such errors contaminate the entire computed scattered wave field. As the computation continues beyond the 15th cycle, the error increases steadily. Ultimately, the numerical solution blows up.

Figure 17 is an identical computation using the optimized extrapolation scheme (with an added constraint). The numerical solution converges to a time period state. There is now excellent agreement between the numerical results and the exact solution. This is, of course, not surprising since the optimized extrapolation as well as the time marching algorithm are designed to yield fairly accurate results for waves with wavelengths of 8 mesh spacings or longer.

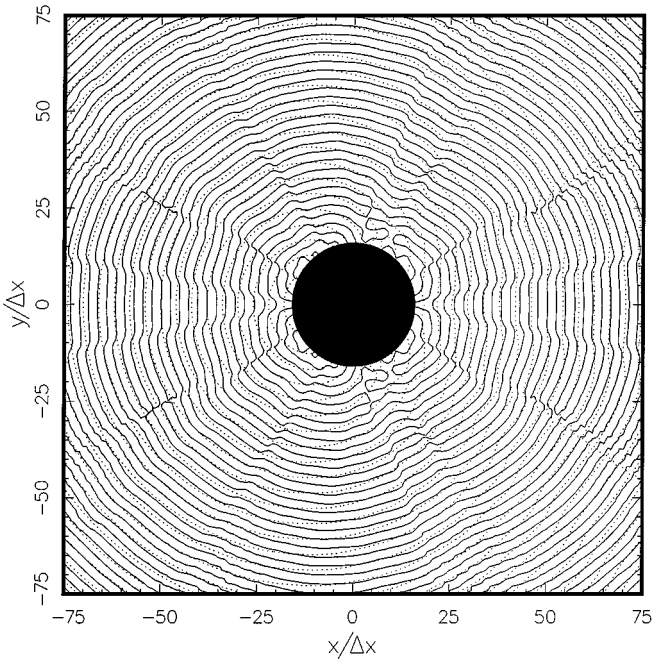

FIG. 16. Zero pressure contours of the scattered sound field at the beginning of a cycle (the 15th cycle from the start of the numerical computation). Lagrange polynomials are used for extrapolation. —, numerical results; . . . , exact solution.

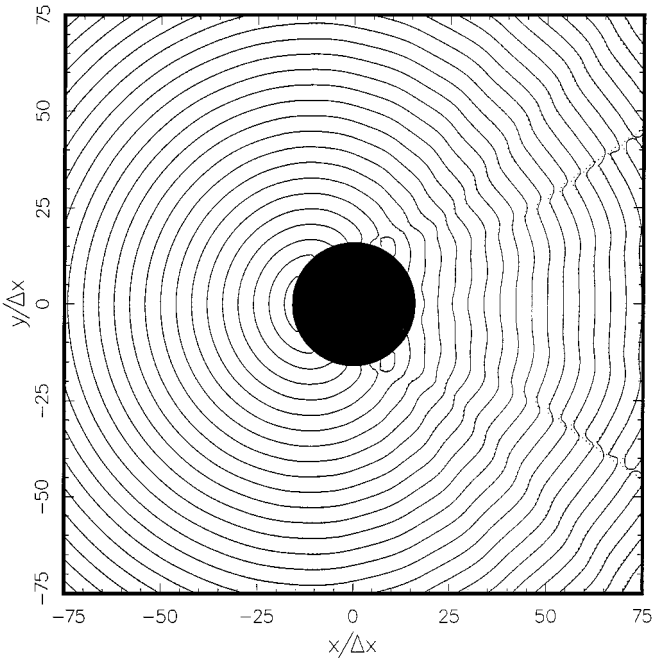

FIG. 17. Zero pressure contours of the scattered sound field at the beginning of a cycle. Optimized extrapolation with added constraint is used. —, numerical results; . . . , exact solution.

5. CONCLUDING REMARKS

In this paper, the errors involved in the application of extrapolation and interpolation are analyzed in the wavenumber space. Standard error analysis, invariably, uses Taylor series expansion and truncation. The error given is usually the first truncated term. Unfortunately, this term cannot often be evaluated, so that there is, in reality, no quantitative information on the error. In contrast, the present wavenumber analysis directly provides the extrapolation and interpolation error distribution as a function of wavenumber. This allows one to make an accurate assessment of the error contribution by such a process apart from the other sources of error in a large scale computation.

In this work, an optimized extrapolation and interpolation method is proposed. The optimization is carried out over a large band of low wavenumbers. When used in conjunction with large scale, high-order finite difference simulations, this band of wavenumbers should be chosen to be the same as the band of the resolved waves of the computation scheme. It is well known that extrapolation often leads to numerical instability. Here it is suggested that such numerical instability is the result of large error amplification over the high wavenumber range. To reduce the tendency to induce numerical instability, the optimized method is extended to include an additional constraint in the optimization process. The added constraint is designed to suppress large error amplification over the high wavenumbers. A numerical example is provided to demonstrate that the new extrapolation method does not lead to numerical instability whereas the use of the more familiar Lagrange polynomials extrapolation method would.

The discussions in this paper have concentrated primarily on the error and numerical instability of extrapolation and interpolation. When used in a specific application or problem, special requirements may sometimes arise. To take into account such special requirements, one may cast them into additional constraints. These constraints can then be incorporated into the optimization process by which the coefficients of the extrapolation formula are determined. This would provide tailor-made accurate and efficient extrapolation and interpolation formulas for specific applications.

APPENDIX: BOUNDARY INSTABILITY DUE TO EXTRAPOLATION

The dimensionless linearized Euler equations that govern the propagation and reflection of acoustic waves are

$$\frac{\partial u}{\partial t} + \frac{\partial p}{\partial x} = 0 \tag{A1}$$

$$\frac{\partial p}{\partial t} + \frac{\partial u}{\partial x} = 0. \tag{A2}$$

The wall boundary condition is

$$x = \eta, \qquad u = 0. \tag{A3}$$

For $\ell \leq -3$ (see Fig. 2), the semi-discretized forms of (A1) and (A2) using a 7-point standard central difference stencil are

$$\frac{du_\ell}{dt} = -\sum_{j=-3}^{3} a_j p_{\ell+j}, \qquad a_{-j} = -a_j \tag{A4}$$

$$\frac{dp_\ell}{dt} = -\sum_{j=-3}^{3} a_j u_{\ell+j}. \tag{A5}$$

In the wall boundary region, $\ell \geq -2$, standard backward difference stencils are used. On discretizing (A1) and (A2), the governing finite difference equations in the boundary region, accounting for the ghost value of p at $\ell = 1$, are

$$\frac{du_{-2}}{dt} = -\sum_{j=-3}^{3} a_j p_{j-2} \tag{A6}$$

$$\frac{dp_{-2}}{dt} = -\sum_{j=-4}^{2} a_j^{42} u_{j-2} \tag{A7}$$

$$\frac{du_{-1}}{dt} = -\sum_{j=-4}^{2} a_j^{42} p_{j-1} \tag{A8}$$

$$\frac{dp_{-1}}{dt} = -\sum_{j=-5}^{1} a_j^{51} u_{j-1} \tag{A9}$$

$$\frac{du_0}{dt} = -\sum_{j=-5}^{1} a_j^{51} p_j \tag{A10}$$

$$\frac{dp_0}{dt} = -\sum_{j=-6}^{0} a_j^{60} u_j, \tag{A11}$$

where a_j^{42}, a_j^{31}, and a_j^{60} are the standard backward difference coefficients for a 6th order scheme. For the wall boundary condition, (A3), the value of u at $x = \eta$ is to be obtained by extrapolation from the nearest 7 mesh points. It may be written as

$$\sum_{j=0}^{6} u_{-j} S_j(\eta) = 0. \tag{A12}$$

In the case where the Lagrange polynomials are used for extrapolation, the extrapolation coefficients, $S_j(\eta)$, are the values of the Lagrange polynomials evaluated at η, that is, $S_j(\eta) = \ell_j^{(7)}(\eta)$.

To investigate the stability of the system (A4) to (A12), we may take the time dependence to be of the form $e^{-i\omega t}$ where ω is the complex angular frequency. The system is unstable or the solution grows exponentially in time if $\mathrm{Im}(\omega) > 0$. Let

$$\begin{bmatrix} p_\ell(t) \\ u_\ell(t) \end{bmatrix} = \begin{bmatrix} \hat{p}_\ell \\ \hat{u}_\ell \end{bmatrix} e^{-i\omega t}. \tag{A13}$$

Substitution of (A13) into (A4) to (A12) leads to the following system of finite difference equations,

$$\ell \leq -3, \qquad i\omega\, \hat{u}_\ell = \sum_{j=-3}^{3} a_j\, \hat{p}_{\ell+j} \tag{A14}$$

$$i\omega\hat{p}_\ell = \sum_{j=-3}^{3} a_j\,\hat{u}_{\ell+j} \tag{A15}$$

$$\ell \geq -2, \qquad i\omega\hat{u}_{-2} = \sum_{j=-3}^{3} a_j\,\hat{p}_{j-2} \tag{A16}$$

$$i\omega\hat{p}_{-2} = \sum_{j=-4}^{2} a_j^{42}\,\hat{u}_{j-2} \tag{A17}$$

$$i\omega\hat{u}_{-1} = \sum_{j=-4}^{2} a_j^{42}\,\hat{p}_{j-1} \tag{A18}$$

$$i\omega\hat{p}_{-1} = \sum_{j=-5}^{1} a_j^{51}\,\hat{u}_{j-1} \tag{A19}$$

$$i\omega\hat{u}_0 = \sum_{j=-5}^{1} a_j^{51}\,\hat{p}_j \tag{A20}$$

$$i\omega\hat{p}_0 = \sum_{j=-6}^{0} a_j^{60}\,\hat{u}_j \tag{A21}$$

$$\sum_{j=0}^{6} \hat{u}_{-j}\,S_j(\eta) = 0. \tag{A22}$$

Finite difference equations (A14) and (A15) can be solved exactly (see Tam, Fang, and Kurbatskii [25]) by letting

$$\begin{bmatrix} \hat{p}_\ell \\ \hat{u}_\ell \end{bmatrix} = \begin{bmatrix} \tilde{p} \\ \tilde{u} \end{bmatrix} e^{i\beta\ell}, \tag{A23}$$

where $\tilde{p}$, $\tilde{u}$, and β are constants. On substituting (A23) into (A14) and (A15) and upon eliminating $\tilde{u}$, it is found

$$(\bar{\beta}^2 - \omega^2)\tilde{p} = 0, \tag{A24}$$

where

$$\bar{\beta} = 2\sum_{j=1}^{3} a_j \sin(\beta j). \tag{A25}$$

For nontrivial solution, $\tilde{p}$ cannot be zero. Equation (A24) yields the following dispersion relations and eigenfunctions

$$\bar{\beta}(\beta) = \omega, \qquad \begin{bmatrix} \tilde{p} \\ \tilde{u} \end{bmatrix} = \begin{bmatrix} 1 \\ 1 \end{bmatrix} \tag{A26}$$

$$\bar{\beta}(\beta) = -\omega, \qquad \begin{bmatrix} \tilde{p} \\ \tilde{u} \end{bmatrix} = \begin{bmatrix} 1 \\ -1 \end{bmatrix}. \tag{A27}$$

It is noted that, by (A25), $\bar{\beta}(-\beta) = -\bar{\beta}(\beta)$.

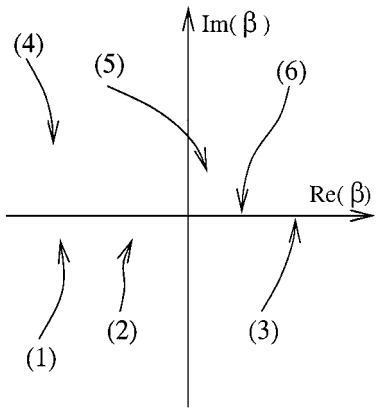

FIG. 18. Trajectories of the six roots of $\bar{\beta}(\beta) = \omega$ in the complex β-plane as ω is pushed toward the real ω-axis in the upper half of the complex ω-plane.

For a given ω, each of the dispersion relations $\bar{\beta}(\beta) = \pm\omega$ has six independent roots. Let those corresponding to $\bar{\beta}(\omega) = \omega$ be $\beta_j(\omega)$, $j = 1, 2, 3, \ldots, 6$. Three of those roots represent waves propagating to the left and the other three propagating to the right. Briggs [26] has developed a procedure to identify the direction of propagation of each of the roots (see also Tam and Dong [21]). Essentially, for the dispersion relation $\bar{\beta}(\beta) = \omega$, one starts by setting the value of ω in the upper half ω-plane with a large imaginary part. The six roots are then found. Three of the roots, β_1, β_2, and β_3, lie in the lower half of the complex β-plane whereas β_4, β_5, and β_6 lie in the upper half β-plane as shown in Fig. 18. It can be shown as ω is pushed toward the real ω-axis, the roots remain in the same half of the β-plane. By the causality condition, the three solutions corresponding to the roots in the lower half β-plane represent waves propagating in the negative x-direction. The other three solutions represent waves propagating in the positive x-direction. By the relationship $\bar{\beta}(-\beta) = -\bar{\beta}(\beta)$, the three roots of the dispersion relation $\bar{\beta}(\beta) = -\omega$ which give rise to wave solutions propagating in the negative x-direction are $-\beta_4$, $-\beta_5$, and $-\beta_6$. Therefore, the general solution of finite difference equations (A14) and (A15) for $\ell \le -3$ satisfying the outgoing wave condition is

$$\begin{bmatrix} \hat{p}_\ell \\ \hat{u}_\ell \end{bmatrix} = c_1 \begin{bmatrix} 1 \\ 1 \end{bmatrix} e^{i\beta_1 \ell} + c_2 \begin{bmatrix} 1 \\ 1 \end{bmatrix} e^{i\beta_2 \ell} + c_3 \begin{bmatrix} 1 \\ 1 \end{bmatrix} e^{i\beta_3 \ell} + c_4 \begin{bmatrix} 1 \\ -1 \end{bmatrix} e^{-i\beta_4 \ell}$$
$$+ c_5 \begin{bmatrix} 1 \\ -1 \end{bmatrix} e^{-i\beta_5 \ell} + c_6 \begin{bmatrix} 1 \\ -1 \end{bmatrix} e^{-i\beta_6 \ell}, \tag{A28}$$

where c_j, $j = 1, 2, \ldots, 6$, are constants.

Now if we replace $\hat{p}_\ell$ and $\hat{u}_\ell$ for $\ell = -3, -4, -5, -6$ in (A14) to (A22) by (A28), we obtain a linear algebraic system of thirteen equations for the thirteen unknowns $c_1, c_2, \ldots, c_6$, $\hat{p}_{-2}, \hat{p}_{-1}, \hat{p}_0, \hat{p}_1, \hat{u}_{-2}, \hat{u}_{-1}, \hat{u}_0$. For nontrivial solution, the determinant of the matrix system, $\Delta(\omega)$, must be equal to zero; i.e.,

$$\Delta(\omega) = 0. \tag{A29}$$

The roots of (A29) provide the eigenvalues of ω. Of interest is whether there is any root of ω with a positive imaginary part. Such a root constitutes an unstable mode. This boundary

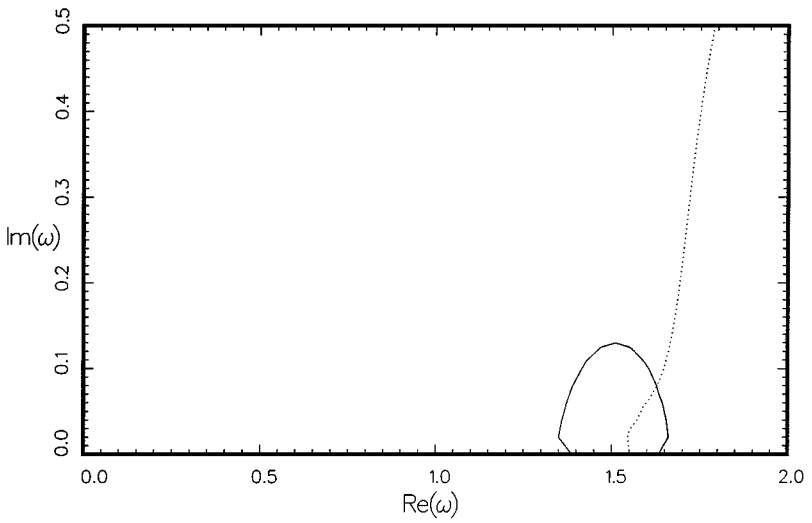

FIG. 19. Grid search for unstable solutions in the complex ω-plane. —, zero contour of the real part of the determinant; . . . , zero contour of the imaginary part of the determinant. $\eta = 0.45$.

instability mode is a spurious solution of the physical problem. It arises from the finite difference approximation and the extrapolation formula. The roots of (A29) can only be determined numerically. A simple way is to use the grid search method of Tam and Hu [27]. On following this method, the contours of $\mathrm{Re}[\Delta(\omega)] = 0$ and $\mathrm{Im}[\Delta(\omega)] = 0$ in the complex ω-plane are constructed. The intersection points of these two sets of contours in the ω-plane give the roots of (A29).

Obviously, the roots of (A29) are influenced by the coefficients of the extrapolation formula, $S_j(\eta)$, of (A22). Figure 19 shows the $\mathrm{Re}[\Delta(\omega)] = 0$ and $\mathrm{Im}[\Delta(\omega)] = 0$ contours in the ω-plane for the case when the Lagrange polynomials are used for extrapolation. Clearly, at $\eta = 0.45$ there is an unstable mode. The frequency ω_r and growth rate ω_i of this instability as a function of the distance of the wall to the first mesh point, η, are given in Fig. 3. For η smaller than 0.42, there is no root of (A29) lying in the upper half ω-plane. In other words, the system is stable. Now if the optimized extrapolation with an added constraint method is used in (A22), no unstable root of (A29) could be found for $\eta \leq 1.0$. This was confirmed by extensive direct numerical solutions of the system of equations (A4) to (A12). This is an important example. It shows that extrapolation can trigger numerical instability. At the same time, it also demonstrates that by using an improved extrapolation procedure such numerical instability can be avoided.

ACKNOWLEDGMENTS

This work was supported in part by NASA Grants NAG 1–1986, NAG 1–2145, and NAG 3–2102. Support by the Florida State University and the Supercomputer Research Institute through the allocation of supercomputer and SP2 resources is hereby acknowledged.

REFERENCES

1. D. Stanescu and W. G. Habashi, Essentially nonoscillatory Euler solutions on unstructured mesh using extrapolation, *AIAA J.* **36**, 1413 (1998).

2. A. Suresh and P. C. E. Jorgenson, *Essentially Nonoscillatory (ENO) Reconstruction via Extrapolation*, AIAA Paper 95-0467, 1995.
3. C. B. Jensen and P. A. Weinerfelt, Coarse grid correction scheme for implicit multiblock Euler calculations, *AIAA J.* **33**, 1816 (1995).
4. S. Chakravarthy, High resolution upwind formulations for the Navier–Stokes equations, in *Proc. VKI Lecture Series 1988-05* (Von Karmen Institute of Fluid Dynamics, Brussels, Belgium, 1989), p. 58.
5. J. Nordstrom, Extrapolation procedures for the time-dependent Navier–Stokes equations, *AIAA J.* **30**, 1654 (1992).
6. J. Nordstrom, Accurate solution of the Navier–Stokes equations despite unknown outflow boundary data, *J. Comput. Phys.* **120**, 184 (1995).
7. Y. T. Jiang, M. Damodaran, and K. H. Lee, High resolution finite volume computation of turbulent transonic flow past airfoils, *AIAA J.* **35**, 1134 (1997).
8. R. A. Johnson and D. M. Belk, Multigrid approach to overset grid communication, *AIAA J.* **33**, 2305 (1995).
9. M. E. Hayder and E. Turkel, Nonreflecting boundary conditions for jet flow computations, *AIAA J.* **33**, 2264 (1995).
10. J. L. Steger and J. A. Benek, On the use of composite grid schemes in computational aerodynamics, *Comput. Methods Appl. Mech. Eng.* **64**, 301 (1987).
11. M. J. Berger and J. Oliger, Adaptive mesh refinement for hyperbolic partial differential equations, *J. Comput. Phys.* **53**, 484 (1984).
12. C. F. Ollivier-Gooch, Multigrid acceleration of an upwind Euler solver on unstructured meshes, *AIAA J.* **33**, 1822 (1995).
13. F. Liu and S. Ji, Unsteady flow calculations with a multigrid Navier–Stokes method, *AIAA J.* **34**, 2047 (1996).
14. C. Sheng, L. K. Taylor, and D. L. Whitfield, Multigrid algorithm for three-dimensional incompressible high-Reynolds number turbulent flows, *AIAA J.* **33**, 2073 (1995).
15. K. H. Kao and M. S. Liou, Advances in overset grid schemes: From Chimera to DRAGON grids, *AIAA J.* **33**, 1809 (1995).
16. K. H. Kao, M. S. Liou, and C. Y. Chow, Grid adaptation using Chimera composite overlapping meshes, *AIAA J.* **32**, 942 (1994).
17. G. Chesshire and W. D. Henshaw, Composite overlapping meshes for the solution of partial differential equations, *J. Comput. Phys.* **90**, 1 (1990).
18. J. A. Wright and W. Shyy, A pressure-based composite grid method for the Navier–Stokes equations, *J. Comput. Phys.* **107**, 225 (1993).
19. D. A. Kopriva and J. H. Kolias, A conservative staggered-grid Chebyshev multidomain method for compressible flows, *J. Comput. Phys.* **125**, 244 (1996).
20. S. D. Conte and C. de Boor, *Elementary Numerical Analysis: An Algorithmic Approach* (McGraw–Hill, New York, 1980).
21. C. K. W. Tam and Z. Dong, Wall boundary conditions for high order finite difference schemes in computational aeroacoustics, *J. Theoret. Comput. Fluid Dynam.* **6**, 303 (1994).
22. C. K. W. Tam and J. C. Webb, Dispersion-relation-preserving finite difference schemes for computational acoustics, *J. Comput. Phys.* **107**, 262 (1993).
23. C. K. W. Tam, Computational aeroacoustics: Issues and methods, *AIAA J.* **33**, 1788 (1995).
24. K. A. Kurbatskii and C. K. W. Tam, Cartesian boundary treatment of curved walls for high-order computational aeroacoustics schemes, *AIAA J.* **35**, 133 (1997).
25. C. K. W. Tam, J. Fang and K. A. Kurbatskii, Non-homogeneous radiation and outflow boundary conditions simulating incoming acoustic and vorticity waves for exterior computational aeroacoustic problems, *Int. J. Numer. Methods Fluids* **26**, 1107 (1998).
26. R. J. Briggs, *Electron-Stream Interaction with Plasmas* (MIT Press, Cambridge, MA, 1964).
27. C. K. W. Tam and F. Q. Hu, Three families of instability waves of high speed jets, *J. Fluid Mech.* **201**, 447 (1989).